Stability of the high-pressure monoclinic phases in Ce and Pr metals: Comparative diffraction study and phenomenological theory

V. P. Dmitriev,[1] A. Yu. Kuznetsov,[1,2] O. Bandilet,[1] P. Bouvier,[3] L. Dubrovinsky,[4] D. Machon,[1,3] and H.-P. Weber[1,2]
[1]*Group "Structure of Material under Extreme Conditions," Swiss-Norwegian Beam Lines at ESRF, Boîte Postale 220, 38043 Grenoble Cedex, France*
[2]*Laboratoire de Cristallographie, EPFL/SB/IPMC/LCR, École Polytechnique Fédéral de Lausanne, CH-1015 Lausanne, Switzerland*
[3]*LEPMI, INPG-CNRS, 1130 rue de la Piscine, Boîte Postale 75, 38402 St. Martin d'Hères Cedex, France*
[4]*Bayerisches Geoinstitut, Universität Bayreuth, D-95440 Bayreuth, Germany*
(Received 8 December 2003; revised manuscript received 25 February 2004; published 16 July 2004)

Pressure-induced structural phase transformations in rare-earth metals Ce and Pr were studied at different temperatures with an externally heated diamond anvil cell by angle dispersive x-ray diffraction using a synchrotron source. Evidence for the presence of the monoclinic $C2/m$ ($Z=8$) phase, Pr-VII, in the pressure range 10–25 GPa has been observed. Theoretical models are proposed and the corresponding phase diagrams are worked out. They are compared to the experimental phase diagrams of cerium and praseodymium. The theory explains consistently the contradictory data on the stability of monoclinic and orthorhombic phases of Ce.

DOI: 10.1103/PhysRevB.70.014104 PACS number(s): 61.50.Ks, 61.66.Bi, 64.70.−p, 71.20.Eh

I. INTRODUCTION

Rare-earth metals exhibit a pronounced systematics in their crystal structures as a function of the atomic number across the lanthanides series or with increasing pressure.[1,2] It is well established that the electron transfer in valence shells induces a characteristic hcp-9*R*-dhcp-fcc-dist.fcc sequence of reconstructive phase transitions in lanthanides[3–5] observed in high-pressure experiments. However, the knowledge about another typical sequence of phase transformations, dist-fcc-monoclinic- "α-*U*"-bct, with some features commonly attributed to phenomena from *f* electrons, is more limited. It has been shown that the "distorted fcc" phase of Pr, found also in La, Nd, Pm, Sm, Gd, and Yb,[6] has a rhombohedral structure ($R\bar{3}m$, $Z=8$) (Ref. 7) and results from a weakly first-order phase transformation from the fcc phase with increasing pressure. The subsequent high-pressure phase reported for Pr, also found in Nd and Sm, has been claimed to be a monoclinic α''-Ce-like structure, which is the precursor of the collapsed phases in these metals.[8,9] The phase transition to the "α-*U*" phase in Pr is commonly considered as an analog of the γ-α isostructural phase transformation in Ce (Refs. 10 and 11) because of the big volume jump involved, thus suggesting a similar electronic phenomenon driving the transformation. At the same time either or both monoclinic and α-*U* phases can be present in the high-pressure sequence of phases in Ce metal, and conflicting evidence with regard to whether one or the other phase is the real equilibrium phase in this metal has been reported (see Ref. 12 and references hereafter).

The structural similitude reported for the high-pressure monoclinic and α-*U* polymorph modifications of Pr and Ce metals motivated us to study more thoroughly the evolution of the above phases as a function of pressure in these metals. The presence of monoclinic and/or α-*U* phases in the phase diagram of Pr and Ce can be comprehensively accounted for in the framework of a phenomenological theory,[13] showing that specific strain/stress conditions induced in the material, for example by the thermomechanical treatment, promote metastable phases in Pr and Ce metals, in agreement with the experimental results.[12]

The format of this paper is as follows. First, after an introduction and presentation of the experimental setup, we communicate, in Sec. III, the results of an accurate diffraction study of the high-pressure–high-temperature phase transformations in Ce and Pr metals, and we discuss important details of their structure parameter behavior indicating the state of *f* electrons in different phases. Then, in Sec. IV, a phenomenological theory is presented which describes the phase diagrams of Ce and Pr and makes consistent the contradictive data published earlier on the stability of monoclinic and orthorhombic phases of Ce.

II. EXPERIMENT

Small chips from polycrystalline Ce and Pr lumps with a purity of 99.9% (GoodFellow) were studied in an externally heated diamond-anvil cell (DAC) by angle-dispersive x-ray-diffraction techniques. *In situ* high-pressure diffraction data were obtained at the ID-30 beam line of the European Synchrotron Radiation Facility (ESRF, Grenoble, France) using monochromatic ($\lambda=0.3738$ Å) *x* radiation. We collected also high-pressure diffraction data from Pr at longer x-ray wavelength ($\lambda=0.72$ Å) at the Swiss-Norwegian Beam Lines (BM 1A, ESRF). Diffraction patterns were collected with an image plate detector (MAR 345). The sample-to-detector distance and the image plate inclination angles were precisely calibrated using a silicon standard. The two-dimensional diffraction images were analyzed using the ESRF FIT2D software, yielding one-dimensional intensity versus diffraction angle 2θ patterns.[14] Rietveld refinement of the structures was performed using the GSAS package.[15] NaCl and ruby provided a pressure calibration. Diffraction mea-

 ©2004 The American Physical Society

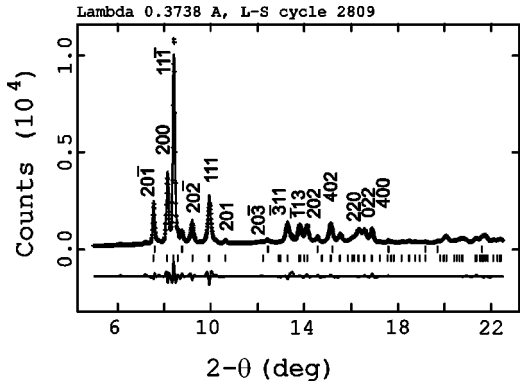

FIG. 1. Diffraction pattern and respective Rietveld fit of α''-Ce at 12.4 GPa with $V=21.851$ Å^3/at. The cross symbols represent experimental data; the solid line running through the data refers to the calculated pattern. The corresponding difference curve is plotted below the diagram. The tick marks indicate the peak positions for the α''-Ce (bottom) and the CeO (top) structures.

surements were performed up to a maximum pressure of 46 GPa in the case of Pr, and up to 22 GPa in experiments with Ce. In order to prevent oxidation, samples were loaded in DAC either with silicon oil or under a dry argon gas atmosphere.

III. RESULTS

A. Cerium

A mixture of dhcp ($P6_3/mmc$, $Z=4$) and fcc ($Fm\bar{3}m$, $Z=1$) phases of Ce, as obtained from the supplier, was transformed into a pure fcc phase, γ, in DAC after loading of the sample without a pressure-transmitting medium and slight compression. In full agreement with the published data, the γ-to-α (fcc-fcc′) isostructural phase transition occurs in Ce in the pressure range 0.6–1.0 GPa. The α-Ce phase then transforms to the monoclinic α''-Ce phase ($C2/m$, $Z=2$) starting from 5.3 GPa. Further pressure increase results, at $P=12.5$ GPa, in the appearance of weak diffraction peaks of the body-centered-tetragonal (bct) structure ($I4/mmm$, $Z=1$). The pressure range of the transformation from α''-Ce to bct-Ce extends to 17.7 GPa.

The previously reported monoclinic α''-Ce structure[12] gives a good trial for the Rietveld refinement of the diffraction pattern, as shown in Fig. 1. The traces of contaminating phases can be distinguished in Fig. 1 as well. A structure indexed with the fcc lattice has a lattice parameter close to that reported for the intermediate space between a γ(fcc) and α(fcc′) "int-fcc" structure.[12,16] Some observations suggest that this phase results from the Ce metal oxidation. In our experiments, the int-fcc was seen in all diffraction patterns with a smooth variation of the cubic lattice parameter as a function of pressure. The phase transitions in Ce produce no remarkable effects on the diffraction peaks attributed to this phase. At pressures above the γ-to-α isostructural phase transition, the int-fcc phase was well resolved, and the Birch-Murnaghan equation of state fitted to high-pressure data gives the lattice parameter extrapolated to ambient pressure

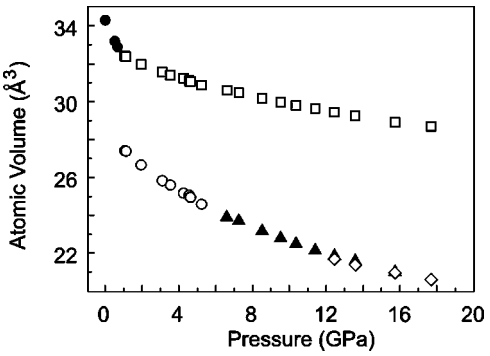

FIG. 2. Atomic volume of Ce metal as a function of increasing pressure. Solid circles, cubic γ-Ce; open circles, cubic α-Ce; triangles, monoclinic α''-Ce; diamonds, tetragonal Ce; squares, CeO.

of 5.092 ± 0.005 Å (see Fig. 2). This value is in good agreement with the lattice parameter $a=5.089$ Å reported for the monoxide CeO, synthesized at high pressure and high temperature.[17] It is worth noting the existence of the metal monoxide already in the "virgin" samples obtained from the supplier. Neither additional oxidation nor any other chemical reaction was observed in our experiments.

The experiments with Ce samples loaded with silicon oil as a pressure-transmitting medium have resulted in an identical sequence of phase transitions with almost the same values of pressures for the phase transformations as in previous experimental conditions. The isostructural γ-to-α phase transition in Ce metal occurs between 1.0 and 2.1 GPa. In this pressure range, silicon oil provides hydrostatic conditions of compression. The high-pressure monoclinic α'' phase appears at 5.8 GPa and then coexists with the bct phase starting from 14.1 GPa. Analogously to nonhydrostatic pressure conditions, weak traces of the same contaminating phases, including int-fcc, were observed on powder diffraction patterns. Both methods of cell loading evidenced no phase with the α-U–type structure in Ce. Figure 2 shows the atomic volume behavior of Ce metal in the studied pressure range.

In order to induce in Ce the transition to the α-U–type phase, as it might follow from the annealing experiments in Ref. 12, we carried out the high-pressure diffraction measurements at elevated temperature. The pressure cell, loaded without a pressure medium, was heated slowly by an external heating element up to 473 K. During the temperature increase, the pressure was kept in the range of 0.3–0.5 GPa. At 0.5 GPa and 473 K, the diffraction pattern exhibits only three strong peaks belonging to γ-Ce.

Subsequent compression at 473 K results, at 1.5 GPa, in the volume-collapsed transition from the γ-Ce phase to the α-Ce one. The single α phase of Ce was stable up to 4 GPa. The image taken at 6 GPa revealed several very intense spots at 2θ values expected for the α-U phase. No traces of α''-Ce phase or any other phase of Ce (except impurities) were detected. The compression of the sample up to 10 GPa induced a gradual distortion of the intense spots from the α-U phase of Ce into the inhomogeneous diffraction rings. We kept the sample at 473 K and 10 GPa for 10 h. No substantial changes were observed in the diffraction patterns during the time of annealing: a single α-U phase of Ce was

present. Such observations correspond to the data of Ref. 12, where the two-phase α''/α-*U* mixture was observed at $P \simeq 7$ GPa and $T=373$ K, while the sample quenched from $P \simeq 10$ GPa and $T=473$ K to $P=5$ GPa and $T=300$ K exhibited a fully transformed α-*U* structure. Our results are therefore in very good agreement with the preceding studies,[4,12,18] and provide a reliable reference for the following experiments with Pr.

B. Praseodymium

The diffraction experiments on Pr disclose the sequence of pressure-induced phases dhcp(Pr-I)–fcc(Pr-II)–dist.fcc(Pr–III). The diffraction peaks from the fcc structure appear at about 5.0 GPa. A two-phase mixture was observed up to 7.7 GPa, where the dhcp-to-fcc phase transformation was completed. The appearance of superlattice reflections characteristic for the rhombohedral phase was clearly seen at 8.1 GPa. The rhombohedral dist.fcc phase ($R\bar{3}m$, $Z=8$) is considered usually to be stable up to about 20 GPa.[7,19] However, we have found that diffraction patterns can be satisfactorily fitted to the corresponding rhombohedral structure only up to about 12 GPa. A systematic and increasing misfit of simulated and experimental diffraction patterns was observed with pressure increasing above 12 GPa. One can see such a difference by comparing the diffraction patterns of Pr and rhombohedral Nd collected at pressures yielding identical atomic volumes [Figs. 3(a) and 3(b), respectively]. It should be noted that the authors of Ref. 20 have also encountered the difficulty of consistently fitting the patterns, near the Pr-III and Pr-IV phase boundary, to known Pr structures.

In search of a trial model for the new phase of Pr, first the monoclinic α''-Ce type structure[8] was discarded [to compare, see Fig. 1 and Fig. 3(a)]. We were unable to index high-pressure diffraction patterns of Pr with this latter structure. A detailed inspection of the diffraction patterns at pressures below and above the transition to the α-*U* phase stable at higher pressure ($P_{tr}=25$ GPa) showed, for example, that the important monoclinic α''-Ce structure reflection $(20\bar{2})$ was not present. Instead, one can observe weak peaks related to the fcc lattice, already mentioned but kept nonindexed by the authors of Ref. 21. We believe that these peaks originate from the monoxide PrO. The high-pressure values of the lattice spacings of the corresponding structure extrapolated to the ambient pressure yield the lattice parameter $a_c=5.029$ Å. This value is in very good agreement with the lattice parameter $a_c=5.031$ Å reported for the PrO structure.[17] It is worth noting also a consistency in the PrO and CeO lattice parameters behavior (Figs. 2 and 4). Again, it should be underlined that no indication of either chemical reaction or oxidation was observed in our experiments with Pr as well.

In order to show more clearly the additional features that distinguish the diffraction patterns of the new structure of Pr and the rhombohedral dist.fcc structure, we carried out high-pressure experiments at longer x-ray wavelength ($\lambda=0.72$ Å). Figure 5 shows the diffraction patterns of Pr in the selected 2θ ranges at different pressures approaching the transition point to the α-*U* phase.

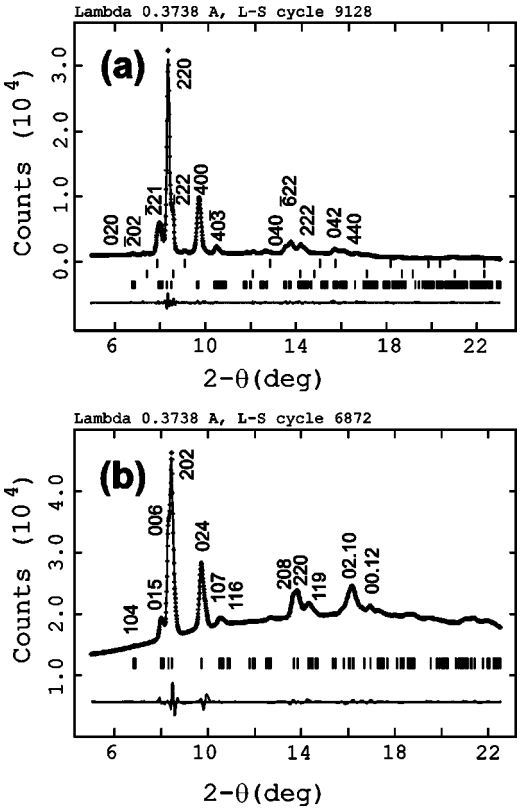

FIG. 3. Diffraction patterns and Rietveld fits of (a) monoclinic structure of Pr described in the text (Pr-VII) at 19.1 GPa with $V=21.969$ Å^3/at compared to (b) rhombohedral dist.fcc structure of Nd at 21.3 GPa with $V=21.414$ Å^3/at. The tick marks in (a) indicate the calculated peak positions for (from bottom to top) Pr-VII, NaCl, and PrO structures.

The most striking effect of increasing pressure on the diffraction pattern of the rhombohedral structure is a variation of the intensity of the (006) and (202) reflections. One can conclude the evident evolution of the corresponding intensity ratio from $I(006)/I(202)<1$ at 13 GPa [Fig. 5(a)] to a reversed $I(006)/I(202)>1$ at 24.9 GPa [Fig. 5(c)]. Neither an increase of the rhombohedral distortion of the fcc phase nor the drastic change in the preferred orientation (which are

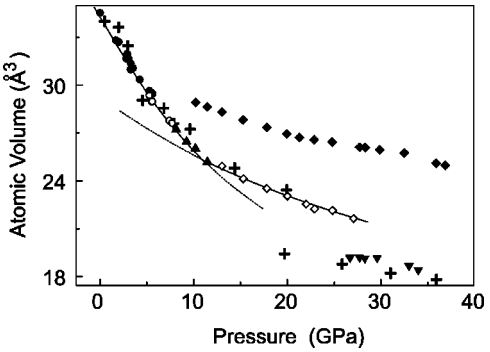

FIG. 4. Atomic volume of Pr metal as a function of increasing pressure: solid circles, dhcp; open circles, fcc; triangles, rhombohedral; open diamonds, monoclinic; inverted triangles, α-*U*; solid diamonds, PrO. Crosses are the data points from Ref. 8.

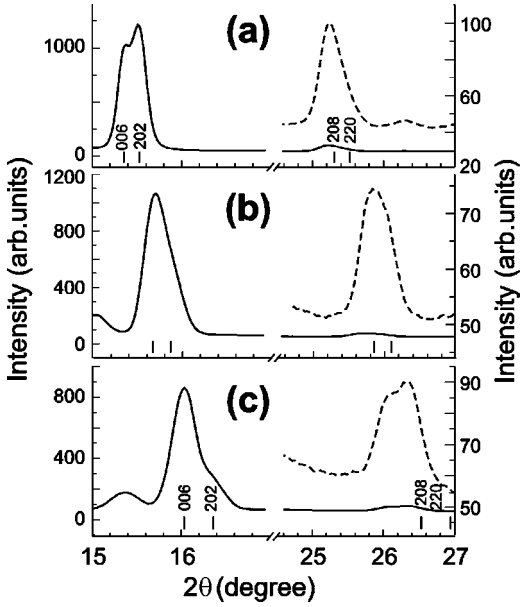

FIG. 5. Diffraction patterns from Pr metal ($\lambda = 0.72$ Å) at increasing pressure: (a) 13.0, (b) 17.8, (c) 24.9 GPa. Solid lines correspond to the left-side intensity scales, dashed lines to the enlarged right-side ones. The tick marks indicate the calculated peak positions for the dist.fcc structure.

necessary to simulate the observed evolution of the intensity ratio) gives a satisfactory full-profile fit. The evident inconsistency relates also to positions of the (208) and (220) rhombohedral lattice reflections as shown in Fig. 5.

The above arguments led us to look for another candidate for the structure of Pr in the pressure range 12–25 GPa. Figure 3(a) shows the experimental diffraction pattern from Pr and the best full-profile fit with the monoclinic structure belonging to the $C2/m$ space group and the unit cell lattice parameters: $a_m = 10.984(2)$ Å, $b_m = 6.3810(2)$ Å, $c_m = 6.275(3)$ Å and $\beta = 126.12(1)°$. The Pr atoms occupy two fourfold positions and one general eightfold position with the atomic positional parameters: $4(i)_1$: (0.7149, 0, 0.2666), $4(i)_2$: (0.2338, 0, 0.2680), and $8(j)$: (−0.0107, 0.7589, 0.2655). At variance with the rhombohedral structure, the above monoclinic one, Pr-VII, gives good reliability indices ($R_{wp} = 0.0383$, goodness of fit equal to 1.62) even without a preferred orientation correction.[22] Figure 6 compares the embedding of the two monoclinic unit cells, α''-Ce and Pr-VII, into the fcc and bcc lattices.

C. Discussion

Contradictory observations were reported on an intermediate phase located between the dist.fcc and the α-U phase. On the one hand, the authors of Ref. 8 reported the existence in Pr of a phase, stable in the pressure range from 10 to 20 GPa, different from the rhombohedral dist.fcc. The corresponding diffraction patterns were indexed with a good fit to a monoclinic structure based on the $C2/m$ symmetry and lattice parameters $a = 5.995$ Å, $b = 3.182$ Å, $c = 5.633$ Å, and $\beta = 112.12°$ (four atoms per unit cell). However, only d spacings were fitted while the calculated intensities of diffraction

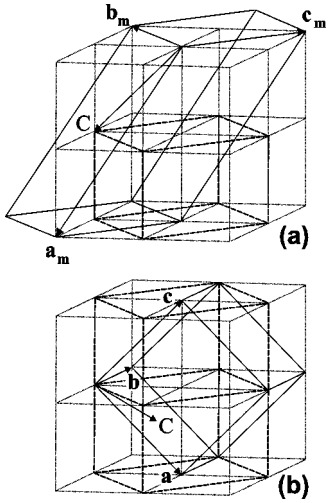

FIG. 6. The relationship between the face-centered (dashed lines), body-centered (dotted lines) cubic lattices, and monoclinic unit cells of Pr-VII (a) and α''-Ce (b). **a**, **b**, and **c** are the basis vectors of the monoclinic Bravais lattice, and **C** is the centered vector. The face-centered-cubic cell is distorted by the reversed Bain deformation.

peaks showed regular deviations from those obtained experimentally.[8] On the other hand, recently published diffraction data,[20] collected at different pressures and temperatures in the same pressure range, showed no evidence of the existence of an intermediate phase. Our high-resolution data provide evidence that a monoclinic phase definitely exists in compressed Pr but its structure is different from the structure suggested in Ref. 8.

An important argument for the existence of a phase transition at $P \simeq 10$ GPa is provided by the equation of state of Pr plotted in Fig. 4 with data obtained in the present study and complemented by data from Ref. 8. One notes, in Fig. 4, an evident singularity at $P \simeq 10$ GPa in the atomic volume dependence plotted versus pressure. The existence of two different compressibilities is a clear indication of a structural change. It is useful also to note that an anomaly in the pressure behavior of the normalized intensity of the (105) superlattice reflection of the dist.fcc phase has already been observed in Pr in the same pressure range.[19]

The question arises as to the existence or the absence of an analogy between monoclinic phases observed in Ce and Pr metals. It is convenient to group the low-pressure phases of Ce into two types, relating to the state of the f electrons: (i) noncollapsed structures in which $4f$ electrons are localized, and (ii) collapsed structures with itinerant $4f$ electrons. The cubic γ-Ce has localized f shells while the other cubic α, monoclinic α'', and orthorhombic α-U structures are considered to be showing electron delocalization effects. The principal indication of the f-electron state transformation in diffraction experiments is the atomic volume collapse observed, for example, at the γ-to-α isostructural phase transition. However, in view of the temperature-induced gradual crossover in Ce through the critical end point of the jumplike delocalization regime to the smooth valence variation regime, it appears more reasonable to underline, in our classification, an itinerant character of the $4f$ electrons themselves

rather than the magnitude of the volume discontinuity (collapse).

An important indication of the *f*-electron state in Pr is provided by the evident change of the Pr structure compressibility at the dist.fcc-to-monoclinic transition (Fig. 4). The almost continuous character of the latter and the preceding fcc-dist.fcc transformation does not allow one to conclude that there is an interatomic nature of such a change, but speaks in favor of the electronic shell modification, which transforms the "compressibility" of the atom itself. One notes the identical values of the bulk modulus, B_0, of monoclinic Ce ($B_0=30.7$ GPa) and Pr ($B_0=30.5$ GPa) metals, both differing remarkably from that of the γ-Ce ($B_0=24.4$ GPa) and fcc Pr-II [$B_0=25.1$ GPa (Ref. 20)] structures. The "collapsed" cubic α-Ce structure yields an intermediate value $B_0=26.7$ GPa. Such an analogy in the "elastic" properties of the Ce and Pr atoms in their monoclinic phases, along with data on the starting valence variation in cubic Pr,[23] leads us to attribute the monoclinic Pr-VII structure to one with already itinerant $4f$ electrons but not to a "precollapsed" structure. The existence of an analogy in the corresponding atomistic mechanisms of the transformations as well will be shown in the following section.

IV. PHENOMENOLOGICAL MODELS

A. Order parameters

As a first step in unifying the preceding crystallographic description of the phases and transformations between them, let us express the basic vectors of the observed low-symmetry monoclinic, orthorhombic, and rhombohedral structures as a function of the basic vectors $\mathbf{a}_i^f$ associated with the fcc lattice. It means that we will consider this latter as the parent phase. Such a choice is justified by the direct adjacent of all low-symmetry phases under consideration with the fcc phase.

From Fig. 6(b), one has for the monoclinic α''-Ce unit cell

$$\mathbf{a}=-\mathbf{a}_2^f+\mathbf{a}_3^f,\quad \mathbf{b}=\mathbf{a}_1^f-\mathbf{a}_2^f,\quad \mathbf{c}=\mathbf{a}_1^f+\mathbf{a}_2^f. \tag{1}$$

The unit cell embedding scheme for the monoclinic Pr-VII [Fig. 6(a)] yields

$$\mathbf{a}_m=-\mathbf{a}_2^f+\mathbf{a}_3^f,\quad \mathbf{b}_m=2(\mathbf{a}_1^f-\mathbf{a}_2^f),\quad \mathbf{c}_m=\mathbf{a}_1^f+\mathbf{a}_2^f. \tag{2}$$

The relationships between basis vectors of the cubic fcc, orthorhombic *a*-*U*, and rhombohedral dist.fcc structures are[13]

$$\mathbf{a}_U=\mathbf{a}_1^f,\quad \mathbf{b}_U=-\mathbf{a}_2^f+\mathbf{a}_3^f,\quad \mathbf{c}_U=\mathbf{a}_2^f+\mathbf{a}_3^f, \tag{3}$$

$$\mathbf{a}_1^R=2\mathbf{a}_1^f,\quad \mathbf{a}_2^R=2\mathbf{a}_2^f,\quad \mathbf{a}_3^R=2\mathbf{a}_3^f. \tag{4}$$

Vectors $\mathbf{a}_1^f=[011]$, $\mathbf{a}_2^f=[101]$, and $\mathbf{a}_3^f=[110]$ in Eqs. (1)–(4) define the *primitive* fcc unit cell.

Following a standard procedure, one can find that order parameter $\{\eta_i\}$ for transformations from the fcc parent phase to Pr-VII, dist.fcc, and α''-Ce belongs to the L point of the fcc Brillouin zone (BZ) characterized by the wave vector $\mathbf{k}_9^f=(\mathbf{b}_1^f+\mathbf{b}_2^f+\mathbf{b}_3^f)/2$ in Kovalev's notation,[24] while the order parameter $\{\xi_i\}$ for the fcc-to-α-*U* transformation belongs to the X point of BZ, characterized by $\mathbf{k}_{10}^f=(\mathbf{b}_1^f+\mathbf{b}_2^f)/2$. The corresponding atomic displacements, distorting the parent phase, represent eigenvectors of the transverse acoustic phonon modes L_3^- and X_5^- or, in the group-theoretical terms, they represent basis functions for the eight-dimensional irreducible representation L_3^- and six-dimensional X_5^- (see, for example, the tables in Ref. 25).

The equilibrium values of the eight-component order parameter (η_i, $i=1$ to 8) describing the considered phases are

$$\text{dist.fcc: } \eta_1/\sqrt{3}=\eta_2=\eta_5/\sqrt{3}=\eta_6=\eta_7/\sqrt{3}=\eta_8=\eta\neq 0,\quad \eta_3=\eta_4=0;$$

$$\alpha''\text{-Ce: } \eta_1\neq 0,\ \eta_j=0\quad (j=2\text{ to }8);$$

$$\text{Pr-VII: } \eta_1=\eta_3=\eta_5=\eta_7=0,\ \eta_j\neq 0\ (j=2,4,6,8). \tag{5}$$

Among the 27 possible low-symmetry equilibrium states, one can find for the X_5^- order parameter (ξ_i, $i=1$ to 6) only one,

$$\xi_1\neq 0,\quad \xi_j=0\quad (j=2\text{ to }6), \tag{6}$$

which corresponds to a phase of orthorhombic symmetry *Cmcm* ($Z=2$), i.e., to the α-*U* phase.[25] By definition, $\eta_i=0$ and $\xi_j=0$ for the fcc phase.

B. Phase diagram for cerium

The introduction of Eqs. (5) and (6), along with transformation properties of the order parameter components (η_i and ξ_i) by the matrices of the irreducible representations L_3^- and X_5^-, respectively, yield the effective Landau free energy for the fcc-to-α''-Ce and fcc-to-α-*U* transitions,

$$F(\eta,\xi)=a_1\eta^2+a_2\eta^4+a_3\eta^6+b_1\xi^2+b_2\xi^4+b_3\xi^6+\gamma_1\eta^2\xi^2, \tag{7}$$

in which the lowest degree biquadratic coupling between single-component effective order parameters η and ξ has been included. The coefficients a_3 and b_3 are assumed to satisfy the conditions $a_3>0$, $b_3>0$, insuring the positive definiteness of $F(\eta,\xi)$ for large values of η and ξ.[26] It is worth noting that the thermodynamic model (7) is "structurally stable," which means it is complete, and the principal predictions concerning the singularity types are valid, even if, for example, the maximal degree of the free-energy expansion is increased.[27] The equations of state corresponding to the potential (7) are

$$\frac{\partial F}{\partial \eta}=2\eta\{a_1+2a_2\eta^2+3a_3\eta^4+\gamma_1\xi^2\}=0,$$

$$\frac{\partial F}{\partial \xi}=2\xi\{b_1+2b_2\xi^2+3b_3\xi^4+\gamma_1\eta^2\}=0. \tag{8}$$

This shows that there are the following four possible equilibrium structures:

$$\text{I: }\eta=0;\ \xi=0\quad :\alpha\text{-Ce(fcc)};$$

$$\text{II: }\eta=0,\ \xi_{1,2}^2=(-b_2\pm\sqrt{b_2^2-3b_1b_3})/3b_3\quad :\alpha\text{-}U;$$

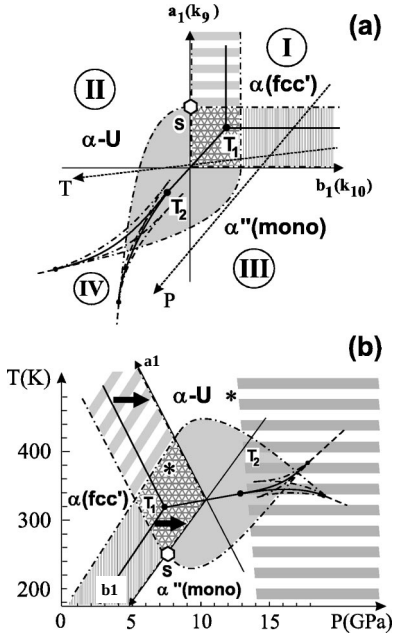

FIG. 7. (a) Phase diagram corresponding to the expansion (7) for $a_2<0$, $b_2<0$, $\gamma_1>0$. Full, dashed, and dash-dotted lines are, respectively, first-order, second-order transition, and limit of stability lines. T_i are three-phase points. Hatched and shadowed areas are the two-phase coexistence regions. The dotted lines show possible *P-T* axes arrangement. (b) The theoretical phase diagram as transformed to the *P-T* coordinate system and compared with experimental data on Ce. Thick arrows represent the data of the present work, asterisks show the points studied by the authors of Ref. 12 and discussed in the text. Striped high-pressure area shows schematically the stability domain of the bct phase.

$$\text{III}: \xi = 0,\ \eta_{1,2}^2 = (-a_2 \pm \sqrt{a_2^2 - 3a_1a_3})/3a_3 \quad : \alpha''\text{-Ce};$$

$$\text{IV}: \eta \neq 0;\ \xi \neq 0 \quad : C2/m(Z=4). \tag{9}$$

The stability domains of the phases listed in Eqs. (9) are determined by the inequalities

$$\begin{vmatrix} \frac{\partial^2 F}{\partial \eta^2} & \frac{\partial^2 F}{\partial \eta\, \partial \xi} \\ \frac{\partial^2 F}{\partial \eta\, \partial \xi} & \frac{\partial^2 F}{\partial \xi^2} \end{vmatrix} = 16\eta^2\xi^2[4(a_2 + 3a_3\eta^2)(b_2 + 3b_3\xi^2) - \gamma_1^2] \geqslant 0,$$

$$\frac{\partial^2 F}{\partial \eta^2} = 8\eta^2(a_2 + 3a_3\eta^2) \geqslant 0. \tag{10}$$

They lead to different phase diagram topologies depending of the signs a_i, b_i, and $\Delta = 4a_2b_2 - \gamma_1^2$.[26] In order to be congruous with the experimental observations, one should choose, for the discussion of Eqs. (8) and (10), the region in which both the fcc-α'' and fcc-α-*U* transformations are of the first order. Figure 7(a) shows the phase diagram corresponding to $a_2<0$, $b_2<0$, $\Delta>0$ in the plane of the coefficients (a_1, b_1), which are assumed to vary linearly as functions of two external variables *T* and *P*,

$$a_1 = \alpha_1(T - T_C) + \alpha_2(P - P_C),$$

$$b_1 = \beta_1(T - T_C) + \beta_2(P - P_C). \tag{11}$$

Note that the three phases (fcc, α-*U*, and α''-Ce) merge at the triple point T_1, and that the α-*U* and α''-Ce phases can be reached from the fcc phase across first-order transition lines. We do not discuss here the region of the phase diagram containing the other triple point, T_2, and two tricritical points since the relating monoclinic phase IV was not found experimentally in lanthanide metals.

The linear transformations (11) convert the diagram of Fig. 7(a) into a *P-T* diagram [Fig. 7(b)], which is more convenient to compare with experimental data. For such an operation we have used (i) data on positions of the two-phase regions fcc/α-*U* and fcc/α''-Ce mapped in our experiments (see above Sec. III) and shown by thick arrows in Fig. 7(b) and (ii) two points from Ref. 12 shown by asterisks. The hatched area on the high-pressure side of the phase diagram of Fig. 7(b) corresponds to the stability domain of a body-centered-tetragonal phase experimentally observed by the authors of Ref. 28. The transformation into this latter is known to be induced by an order parameter different from those considered above.[13] For the sake of simplicity, and without loss of generality, we did not include it in our analysis.

Some comments are needed concerning a *semiquantitative* character of the phase diagram of Fig. 7(b) calculated in the framework of the model (7). First, the model (7) is a thermodynamic one and therefore takes into account no kinetic aspects of the transformations. This means, for example, that the considered model predicts a transformation starting at the pressure and temperature at which the energy of the initial state is equal to the energy of the final state (first-order transition lines in Fig. 7). However, in real systems, due to kinetic reasons, a transition starts at higher pressure and temperature, when these external parameters vary upward. Second, the model (7) is a phenomenological one and needs, in order to be quantitative, a sufficient set of experimental data, which is not the case for the transformations in the Ce metal. Nevertheless, it should be pointed out that all predicted tendencies can be considered to be reliable.

C. Phase diagram for praseodymium

The phenomenological model for Pr turns out to be more complicated than the one for Ce. The equilibrium relationships (5) show that both low-symmetry phases of praseodymium, namely dist.fcc and Pr-VII, are induced by the same order parameter $\{\xi_i\}$. This leads one to conclude that the corresponding *effective* order parameter, in contrast with the model considered in Sec. IV B for Ce, should be at least two-component. The advanced model deals with the effective Landau energy

$$F(\eta, \xi_1, \xi_2) = a_1\eta^2 + a_2\eta^4 + a_3\eta^6 + b_1(\xi_1^2 + \xi_2^2) + b_2(\xi_1^2 + \xi_2^2)^2 + c(\xi_1^4 + \xi_2^4) + b_3(\xi_1^6 + \xi_2^6) + \gamma\eta^2(\xi_1^2 + \xi_2^2). \tag{12}$$

This model was analyzed earlier in Ref. 29. Here we will use some results of that comprehensive consideration. The

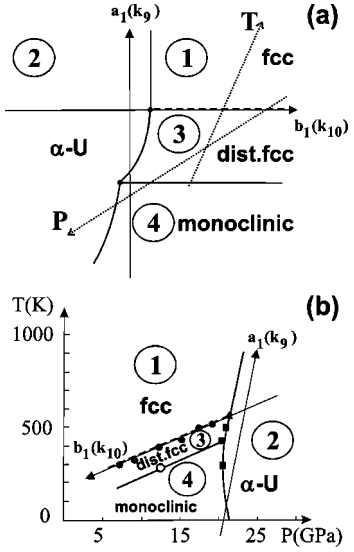

FIG. 8. Equilibrium phase diagrams associated with the order-parameter expansion defined by Eq. (12) for $b_2+c>0$, $c>0$, $\gamma_1>0$. Full, dashed, and dotted lines have the same meaning as in Fig. 7. (a) Theoretical phase diagram; (b) diagram transformed to the *P-T* coordinate system and compared with experimental data from Ref. 11 (solid symbols) and supplemented by the dist.fcc-to-Pr-VII transition point found in the present study (open symbol).

equations of state corresponding to the potential (12) are

$$\frac{\partial F}{\partial \eta} = 2\eta\{a_1 + 2a_2\eta^2 + 3a_3\eta^4 + \gamma(\xi_1^2 + \xi_2^2)\} = 0,$$

$$\frac{\partial F}{\partial \xi_i} = 2\xi_i\{b_1 + 2b_2(\xi_1^2 + \xi_2^2) + 2c\xi_i^2 + 3b_3\xi_i^4 + \gamma\eta^2\} = 0. \tag{13}$$

The system (13) has six solutions, four of which can be identified as the phases observed in Pr,

$$1: \eta = 0;\ \xi_i = 0 \quad \text{:Pr-II (fcc);}$$

$$2: \eta \neq 0,\ \xi_i = 0 \quad \text{:Pr-IV } (\alpha\text{-}U);$$

$$3: \eta = 0,\ \xi_1 \neq 0,\ \xi_2 = 0 \quad \text{:Pr-III (dist.fcc);}$$

$$4: \eta \neq 0;\ \xi_1 = \xi_2 \neq 0 \quad \text{:Pr-VII (monoclinic).} \tag{14}$$

Figure 8(a) represents the phase diagram resulting from the minimization of the potential (12) in the plane of the phenomenological parameters (a_1, b_1), and Fig. 8(b) shows the same diagram converted, making use of the transformation (11), in the *P-T* coordinates. One can conclude that the theoretical diagram reproduces sufficiently well the topology of the experimental diagram of the Pr metal, where the room-temperature sequence of phases fcc-dist.fcc-monoclinic-α-*U* evolves to the fcc-α-*U* sequence at elevated temperature, therefore this latter phase dominates in the phase diagram.[30]

An important point to be mentioned is the compatibility of the partial phase diagram of Fig. 8, calculated in the framework of the model Eq. (12), with the whole phase diagram of Pr including the melting curve.[31] The transition line predicted for the 1(Pr-II)-to-2(Pr-IV) transformation and extrapolated to higher temperatures and pressures intercepts the experimentally determined melting curve close to the triple point melt-fcc-α-*U* suggested by the authors of Ref. 31 at $P \simeq 24$ GPa and $T \simeq 1400$ K.

Another conclusion, worth noting as potentially useful for future microscopic considerations, results from a comparison of the theoretically predicted and experimentally observed character of the dist.fcc-to-Pr-VII phase transition. From our experiments, we have found this transformation to be weakly first-order. In the model (12), the character of this transition can be estimated from the width, σ, of the 3/4 coexistence region, limited by straight lines,[29]

$$3: a_1^{(3)} = \frac{4a_2c}{3b_3},$$

$$4: a_1^{(4)} = \frac{4a_2c - c^2}{3b_3}. \tag{15}$$

By subtracting, one has

$$\sigma = \frac{c^2}{3b_3}. \tag{16}$$

According Eq. (16), the almost continuous character of the 3-4 (Pr-III–to–Pr-VII) phase transformation indicates, for Pr, a vanishing of the phenomenological parameter *c* in the Landau energy (12). σ is equal to zero for the second-order phase transition. One can note the existence, in the potential (12), of two fourth-degree terms: one, b_2, is the squared quadratic invariant; the other, *c*, is the basis invariant itself. In terms of atomic interactions, the first one represents four-particle interactions, which can be reduced to the pairwise (central) ones, while the latter basis invariant represents more complex quadrupolar (noncentral) interactions. The vanishing of the *c* coefficient in the free energy (12) indicates a negligible role of the quadrupolar interatomic forces in the stabilization of the low-symmetry crystal structures in Pr.

D. Strain effect on the monoclinic and orthorhombic phase stability

An important question, which this paper addresses, regards the origin and mechanism of a remarkable elastic field effect on the monoclinic and orthorhombic phase stability in Ce. In the Introduction, we mentioned the controversial situation when one body of literature claims that cubic α-Ce transforms to the α-*U* structure, but another body of work concludes with equal certainty that the transition is to a different, monoclinic structure. The authors of Ref. 12 demonstrated that the conflicting results obtained for the phases above 5 GPa arise from differing methods of sample preparation. They suggested that cold working, if applied to the metal at the preparation stage, somehow favors the small shear distortion, which, in turn, promotes the change in the phase sequence. In this and the following sections we will show, in the framework of the present group-theoretical and

thermodynamic theory, how an elastic field shifts the stability limits of the phases, and explain why this effect is especially pronounced for the α''-Ce/α-U phase boundary.

The strain effect can be foreseen by considering the mixed free-energy expansion

$$\tilde{F}(\eta,\xi,e_i) = F(\eta,\xi) + \frac{1}{2}c_{ij}e_ie_j + \gamma_2\eta^2e_i + \gamma_3\xi^2e_i, \quad (17)$$

where $F(\eta,\xi)$ is the effective order-parameter expansion, given by Eq. (7), associated with the α–α'' and α–α–U phase transitions. The remaining terms in Eq. (17) express the free energy associated with the onset of homogeneous shear strains, e_i, induced by the phase transitions or by an external stress, and the coupling of e_i with the structural order parameters. The elastic energy contribution is restricted to a quadratic term due to its noncritical (nonsymmetry-breaking) character. The form of the coupling terms is determined by the symmetry properties of the primary order parameters η and ξ. Minimization with respect to e_i of $\tilde{F}$ provides the equation of state

$$\frac{\partial\tilde{F}}{\partial e_i} = \gamma_2\eta^2 + \gamma_3\xi^2 + c_{ij}e_j = 0, \quad (18)$$

which yields equilibrium relationships between order parameters and strain components in different phases,

$$e_i^0 = -\frac{\gamma_2\eta^2 + \gamma_3\xi^2}{c_{ij}}. \quad (19)$$

Introducing it in Eq. (17) gives the renormalized form of $\tilde{F}$,

$$\tilde{F}(\eta,\xi) = a_1\eta^2 + \tilde{a}_2\eta^4 + a_3\eta^6 + b_1\xi^2 + \tilde{b}_2\xi^4 + b_3\xi^6 + \tilde{\gamma}\eta^2\xi^2, \quad (20)$$

where

$$\tilde{a}_2 = a_2 - \frac{\gamma_2^2}{2c_{ij}}, \quad \tilde{b}_2 = b_2 - \frac{\gamma_3^2}{2c_{ij}}, \quad \tilde{\gamma} = \gamma_1 - \frac{\gamma_2\gamma_3}{c_{ij}}. \quad (21)$$

In order to simplify our demonstration, let us consider the strain effect on the position of the point S [Fig. 7(b)] where the stability limit (spinodal line) of the α-U phase with respect to the parent fcc phase joins the stability limit with respect to the α''-Ce phase. The strain-induced shift of this point is characteristic, therefore, of both stability limit lines. Equations (10) yield the coordinates of the point S on the phase diagram of a stress-free sample,

$$\left\{a_1^0 = 0, \quad b_1^0 = \frac{b_2^2}{3b_3}\right\}. \quad (22)$$

A stress applied to or induced in the sample displaces this point along the b_1 axis to a new position characterized by the same Eqs. (22) but with the renormalized parameter $\tilde{b}_2$ [see Eq. (21)]. One can find the corresponding shift, δ,

$$\delta = b_1^0(b_2) - b_1^e(\tilde{b}_2) = \frac{\gamma_3}{3c_{ij}b_3}\left\{b_2 - \frac{\gamma_3}{4c_{ij}}\right\}. \quad (23)$$

For a weak repulsive interaction of the order parameter with strains ($\gamma_3 < 0$), δ is positive (remember that $b_2 < 0$, $b_3 > 0$, $c_{ij} > 0$) and the point S is shifted towards the (a_1, b_1) coordinate system origin or, in terms of physically variable parameters, to higher temperatures [Fig. 7(b)]. Completely in accordance with this theoretical prediction, in the course of compressing, a stress-free Ce sample transforms, at room temperature and pressure around 7 GPa, into the α-U phase, while a cold-worked (stressed) one undergoes the fcc-to-α'' transformation. It is worth noting that the above consideration and its conclusions are applicable to Pr as well, since the substitution of the single-component order parameter ξ by the two-component one $\{\xi_{1,2}\}$ in the expansion (17) does not change the principal equations of the corresponding model.

E. Transformation mechanisms and order-parameter genesis

It remains to understand the special sensitivity of the α''-α-U phase boundary with respect to external effects. For this goal, one should analyze, in the framework of an advanced model, the mechanisms of the fcc-α'' and fcc-α-U transformations. The theory developed in the preceding sections for these transformations is a local one, which considers the fcc phase as a parent one. Although it provides an adequate description of the corresponding phase diagrams, a more general unifying description of all the lanthanide structures was proposed earlier in terms of displacive mechanisms occurring from a bcc parent structure.[13] Such a picture was justified by the existence of a bcc phase below the melt in the phase diagrams of at least 11 lanthanide elements.[6] The displacive transformation mechanisms from the bcc structure were divided into two types: (i) variants of the Burgers mechanism[32] which give rise to hcp, dhcp, and 9R structures, and (ii) variants of the Bain deformation mechanism[33] which yield the fcc and bct structures. The monoclinic α''-Ce and orthorhombic α-U structures provide a link between the two preceding variants.

The bcc-hcp Burgers mechanism can be formulated in terms of antiparallel shifting of the atoms lying in the $(110)_{bcc}$ planes along $\pm[\bar{1}10]_{bcc}$ directions. It leads to the orthorhombic α-U-type structure (space group $Cmcm$, $Z=2$), which transforms into the hcp structure for the special shifts, supplemented by spontaneous deformations consisting in tensile and shear strains.[34] The bcc-fcc Bain deformation consists in stretching the bcc unit cell along one of the fourfold axes and compressing along the other fourfold axes.

Let us consider the interaction of the above two mechanisms destabilizing the bcc parent structure. The primary order parameter, which corresponds to the Burgers mechanism, belongs to the point N_b (vector $\mathbf{k}_9^b = \mathbf{b}_3^b/2$) of the bcc BZ, and spans the six-dimensional irreducible representation N_4^-. Condensation of a single OP component (for example, $\eta_1 \neq 0$, $\eta_{2\text{ to }6} = 0$) induces the bcc-α-U structure transformation,[13,34] which reduces the crystal class order by factor 6: $[m\bar{3}m]/[mmm] = 48/8 = 6$. At the onset, this latter

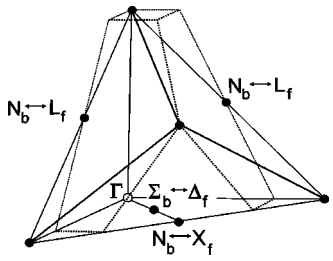

FIG. 9. Geometrical connection between the N_b point of the bcc BZ (solid lines) and the X_f and L_f points of the fcc BZ (dotted lines; the Bain deformation is not applied).

reduction results, in the crystal, in six orientational domains of the orthorhombic phase, each corresponding to different single $\eta_i \neq 0$. The coincidence of the symmetry group *mmm* of the vector $\mathbf{k}_9^b$ and the crystal class of the low-symmetry structure allows one to relate every orientational domain of the α-*U* phase to the corresponding arm of the star $\{\mathbf{k}_9^{(i)}\}$ or to the corresponding single point of the sixfold N_b position. In the Ce metal, such destabilization of the bcc structure is forestalled by the distortion of the crystal with the Bain deformation mechanism, transforming the bcc structure to the fcc one. In the reciprocal space, the Bain deformation "splits" the sixfold N_b-point position of the bcc BZ to two, L_f and X_f, in the fcc BZ (Fig. 9). This means that the single transformation channel from the bcc structure to the α-*U* structure branches, under the effect of the Bain deformation, into two nonequivalent channels, i.e., the single Burgers instability appears as two different instabilities if it is considered in terms of the fcc structure. The straightforward group-theoretical procedure allows one to conclude that the final product of the transformation, appearing as one induced by an order parameter from the X_f point, is the α-*U* structure, while the other one, resulting from the instability in the L_f point, is the α''-Ce structure. In the other words, α-*U* and α''-Ce structures are the originally equivalent domains of the same orthorhombic phase distorted, due to its different orientation, in a different manner by the "external field" of the second order parameter (Bain deformation). The α-*U*–to–α''-Ce structure transformation appears, therefore, as a type of switching of domains. Such an interpretation of the α-U–α'' transformation character reasonably justifies the existence of such a low energetic barrier for the transformation process and, consequently, its elevated sensitivity with respect to external effects. The mechanism of the *elastic* field effect was considered in the preceding section.

V. CONCLUSIONS

Our x-ray-diffraction study definitely evidenced the existence of the monoclinic $C2/m$ $(Z=8)$ phase, Pr-VII, in the pressure range 10–25 GPa, intermediate between the distorted fcc, Pr-III, and the orthorhombic, Pr-IV, phases. The symmetry analysis shows that the same phonon L_3^- instability as for the fcc-dist.fcc and fcc-α''-Ce transformations induces the transition into the monoclinic Pr-VII phase. The phenomenological models proposed for the preceding transformations reproduce well the topology of the phase *P-T* diagrams of Ce and Pr, and relate the high lability of the α''-Ce/α-*U* phase boundary to the identity of their distortion mechanisms.

ACKNOWLEDGMENTS

Experimental assistance from the staff of ID30 and the Swiss-Norwegian Beam Lines at ESRF is gratefully acknowledged. Dr. T. Le Bihan is thanked for the fruitful discussions.

[1] B. Johansson and A. Rosengren, Phys. Rev. B **11**, 2836 (1975).
[2] W. B. Holzapfel, J. Alloys Compd. **223**, 170 (1995).
[3] J. C. Duthie and D. G. Pettifor, Phys. Rev. Lett. **38**, 564 (1977).
[4] A. K. McMahan and D. A. Young, Phys. Lett. **105A**, 129 (1984).
[5] H. L. Skriver, Phys. Rev. B **31**, 1909 (1985).
[6] D. A. Young, *Phase Diagrams of the Elements* (Univ. California Press, Berkeley, 1991).
[7] N. Hamaya, Y. Sakamoto, H. Fujihisa, Y. Fujii, K. Takemura, T. Kikegawa, and O. Shimomura, J. Phys.: Condens. Matter **5**, L369 (1993).
[8] G. N. Chesnut and Y. K. Vohra, Phys. Rev. B **62**, 2965 (2000).
[9] J. Akella, S. T. Weir, Y. K. Vohra, H. Prokop, S. A. Catledge, and G. N. Chesnut, J. Phys.: Condens. Matter **11**, 6515 (1999).
[10] H. K. Mao, R. M. Hazen, and P. M. Bell, J. Appl. Phys. **52**, 4572 (1981).
[11] Y. C. Zhao, F. Porsch, and W. B. Holzapfel, Phys. Rev. B **52**, 134 (1995).
[12] M. I. McMahon and R. J. Nelmes, Phys. Rev. Lett. **78**, 3884 (1997).
[13] V. P. Dmitriev, A. Yu. Kuznetsov, D. Machon, H.-P. Weber, and P. Tolédano, Europhys. Lett. **61**, 783 (2003).
[14] A. P. Hammersley, S. O. Svensson, M. Hanfland, A. N. Fitch, and D. Hausermann, High Press. Res. **14**, 235 (1996).
[15] A. C. Larson and R. V. Von Dreele, *GSAS Technical Manual* (Los Alamos National Laboratory, Los Alamos, 1985–2000).
[16] K. A. Gschneidner, R. O. Elliot, and R. R. McDonald, J. Phys. Chem. Solids **23**, 555 (1962).
[17] J. M. Léger, N. Yacoubi, and J. Loriers, J. Solid State Chem. **36**, 261 (1981).
[18] L. S. Olsen, L. Gerward, U. Benedict, and J.-P. Itié, Physica B & C **133B**, 129 (1985).
[19] W. A. Grosshans, Y. K. Vohra, and W. B. Holzapfel, Phys. Rev. Lett. **49**, 1572 (1982).
[20] B. J. Baer, H. Cynn, V. Iota, C. S. Yoo, and G. Shen, Phys. Rev. B **67**, 134115 (2003).
[21] N. Hamaya, Y. Sakamoto, H. Fujihisa, Y. Fujii, K. Takemura, T. Kikegawa, and O. Shimomura, in *High Pressure Science and Technology—1993*, edited by S. C. Schmidt *et al.*, AIP Conf. Proc. No. 309 (AIP, New York, 1994), Pt. 1, p. 457.
[22] F. Porsch and W. B. Holzapfel, Phys. Rev. B **50**, 16 212 (1994).

[23] A. Yu. Kuznetsov, V. P. Dmitriev, O. I. Bandilet, and H.-P. Weber, Phys. Rev. B **68**, 064109 (2003).
[24] O. V. Kovalev, *Irreducible Representations of the Space Groups* (Gordon and Breach, New York, 1965).
[25] H. T. Stokes and D. M. Hatch, *Isotropy Subgroups of the 230 Crystallographic Space Groups* (World Scientific, Singapore, 1988).
[26] Yu. M. Gufan and E. S. Larin, Sov. Phys. Solid State **22**, 270 (1980) [Fiz. Tverd. Tela (Leningrad) **22**, 463 (1980)].
[27] E. T. Kut'in, V. L. Lorman, and S. V. Pavlov, Sov. Phys. Usp. **34**, 497 (1991) [Usp. Fiz. Nauk **191**, 109 (1991)].
[28] A. Schiwek, F. Porsch, and W. B. Holzapfel, High Press. Res. **22**, 407 (2002).
[29] E. S. Larin, Sov. Phys. Solid State **26**, 1820 (1984) [Fiz. Tverd. Tela (Leningrad) **26**, 3019 (1984)].
[30] We mapped data from Ref. 11 but not recently published (Ref. 20) since these latter differ considerably from the data published earlier, a fact mentioned by the authors of Ref. 20.
[31] D. Errandonea, R. Boehler, and M. Ross, Phys. Rev. Lett. **85**, 3444 (2000).
[32] W. G. Burgers, Physica (Amsterdam) **1**, 561 (1934).
[33] E. G. Bain, Trans. Am. Inst. Min., Metall. Pet. Eng. **70**, 25 (1924).
[34] V. P. Dmitriev, Yu. Gufan, and P. Tolédano, Phys. Rev. B **44**, 7248 (1991).